

# Unusual Function of Modified Polyolefins for Manipulating Magnetic Nanostructures

QINGLIANG HE,<sup>1</sup> TINGTING YUAN,<sup>1</sup> SUYING WEI,<sup>1,2</sup>  
and ZHANHU GUO<sup>1,3</sup>

1.—Integrated Composites Laboratory (ICL), Dan F. Smith Department of Chemical Engineering, Lamar University, Beaumont, TX 77710, USA. 2.—Department of Chemistry and Biochemistry, Lamar University, Beaumont, TX 77710, USA. 3.—e-mail: zhanhu.guo@lamar.edu

The unusual function of a long known plastic additive in industry, polypropylene-*graft*-maleic anhydride (PP-*g*-MA), is reviewed for serving as a polymeric surfactant to synthesize and stabilize magnetic nanoparticles (NPs) with tunable morphology and crystalline structure. The synthesis route employs a solution-based, one-pot, bottom-up method. Specifically, magnetic NPs were synthesized through thermo-decomposing organo-metallic precursors [i.e., Fe(CO)<sub>5</sub> or Co<sub>2</sub>(CO)<sub>8</sub>] in the presence of PP-*g*-MA in solvent xylene. By simply changing the backbone length/concentration of PP-*g*-MA, different morphologies (monodispersed hollow vs. chain-like solid, or chain-like vs. monodispersed polyhedral-shaped NPs) and crystalline structures [ $\alpha$ - vs.  $\gamma$ -phase for Fe<sub>2</sub>O<sub>3</sub> NPs, or face-centered cubic (fcc)- vs.  $\epsilon$ -phase for Co NPs] can be controlled simultaneously. In addition, for the chain-like Fe<sub>2</sub>O<sub>3</sub> NPs, a different chain diameter and building block morphology can be controlled by only varying the molecular weight of PP-*g*-MA.

## INTRODUCTION

Magnetic nanoparticles (NPs) have been extensively studied for a variety of potential applications because of their unique size- and shape-dependent physicochemical properties. The morphology (size and shape) control of magnetic NPs by many small molecular surfactants has been well established<sup>1,2</sup> by varying the binding density/strength of the surfactant(s) on the surface of magnetic NPs.<sup>3,4</sup> In addition, the magnetic properties of these NPs have been considered to be strongly associated with their size, shape, and crystalline phase.<sup>5</sup> Magnetic iron group elements have abundant crystalline structures, both those found in nature and human-made. For example, Fe<sub>2</sub>O<sub>3</sub> has four different crystalline structures ( $\alpha$ -,  $\beta$ -,  $\gamma$ -, and  $\epsilon$ -),<sup>6</sup> whereas cobalt has three (fcc-, hcp-, and  $\epsilon$ -) phases.<sup>7</sup> Hence, extensive efforts have been made for developing simple approaches to control the crystalline structures of these magnetic NPs because the coexistence of two crystalline structures is undesirable. Thereafter, the control of magnetic properties as well as of other physicochemical properties of these magnetic NPs can thus be

targeted to achieve desirable multifunctionalities for specific applications. Among many developed approaches (high-temperature reduction, evaporation–condensation, melting–crystallization, and thermal decomposition), the relative low-temperature solution chemistry is ideal for yielding extensively a one-phase structure with the aid of different capping ligands.<sup>8</sup>

Usually, polymers with polar structures or functional groups in their backbones<sup>9–13</sup> are ideal for serving as surfactants to stabilize magnetic NPs in colloids. These surfactants with different affinity to magnetic NPs can control the growth of a specific crystalline facet or stacking sequence. Hence, magnetic NPs with a desirable crystalline phase can be achieved by adjusting the concentration/composition of different surfactant(s). However, the functionalized polymers have rarely been reported to control the crystalline phase of the magnetic NPs even though the morphology control has been studied. Here, for a well-known modified polyolefin, PP-*g*-MA, whether it is suitable for synthesizing and stabilizing the magnetic NPs is discussed and its unusual function for controlling magnetic nanostructures is reviewed.

## EXPERIMENTAL PROCEDURES

The polypropylene (PP) used here was supplied by Total Petrochemicals USA, Inc ( $M_n \approx 40,500$ ). Polypropylene-*graft*-maleic anhydride (PP-*g*-MA) with three different molecular weights [(1)  $M_n \approx 8000$ ; (2)  $M_n \approx 2500$ ; and (3)  $M_n \approx 800$ ] was provided by Baker Hughes Inc. PP-*g*-MA-1a ( $M_n \approx 8000$ ) is a homo-polypropylene with one terminal and one grafting MA on the PP chain, whereas PP-*g*-MA-1b ( $M_n \approx 8000$ ) is a homo-polypropylene with only one terminal MA on the PP chain. PP-*g*-MA-2 ( $M_n \approx 2500$ ) is a homo-polypropylene with one terminal MA, whereas PP-*g*-MA-3 ( $M_n \approx 800$ ) is a propylene-hexene copolymer with one MA at one terminal and the other MA grafted on the main chain. Iron pentacarbonyl ( $\text{Fe}(\text{CO})_5$ , 99%) was commercially obtained from Sigma Aldrich. Dicobalt octacarbonyl ( $\text{Co}_2(\text{CO})_8$ , stabilized with 1–5% hexane) was obtained from Strem Chemicals, Inc. Solvent xylene (laboratory grade,  $\rho = 0.87 \text{ g/cm}^3$ ) was purchased from Fisher Scientific. All chemicals were used as received without any further treatment.

The detailed synthesis procedures are reported elsewhere.<sup>14–16</sup> Take hollow  $\text{Fe}_2\text{O}_3$  NPs as example: First, 1.0-g PP-*g*-MA and 100-mL xylene were added into a 250-mL three-neck round bottom flask; then the mixture was heated to reflux ( $\sim 140^\circ\text{C}$ ) to dissolve the PP-*g*-MA. Second, the solution was cooled to around  $110\text{--}120^\circ\text{C}$ ; meanwhile, 3.5-g  $\text{Fe}(\text{CO})_5$  was injected into the flask. The solution was immediately turned from transparent to brown and then gradually black during an additional 3-h refluxing process. Finally, the solution was cooled to room temperature in the flask and half of the colloidal solution was used for further measurement

and the rest was poured into a glass container to evaporate the solvent in the fume hood overnight.

## CHARACTERIZATION

The morphology of the as-prepared NPs was studied using a transmission electron microscope (TEM) in a FEI TECNAI G2 F20 microscope at a working voltage of 200 kV. The x-ray diffraction (XRD) analysis was carried out with a Bruker AXS D8 Discover diffractometer with a general area detector diffraction system (GADDS) operating with a  $\text{Cu-K } \alpha$  radiation source filtered with a graphite monochromator ( $\lambda = 1.5406 \text{ \AA}$ ). The magnetic property was measured using a 9 T physical properties measurement system (PPMS) by Quantum Design.

## RESULTS AND DISCUSSION

### The Role of PP-*g*-MA

It is well known that fatty acids are ideal surfactants for synthesizing magnetic NPs using the bottom-up method because the carboxylic groups on one end of the fatty acid have strong affinity to small metal clusters,<sup>17</sup> which can coordinate the growth of magnetic NPs in a controllable manner; meanwhile, the long alkyl chain of the fatty acid can provide steric hindrance to separate the easy self-agglomerated magnetic NPs. Similarly, the maleic anhydride in the PP-*g*-MA has such advantage comparable to the fatty acids; the carboxylic groups can be formed upon the hydrolysis of PP-*g*-MA, so that the carboxylic groups can further be used to bind the magnetic NPs. In addition, the PP tail can provide steric hindrance to isolate the magnetic NPs

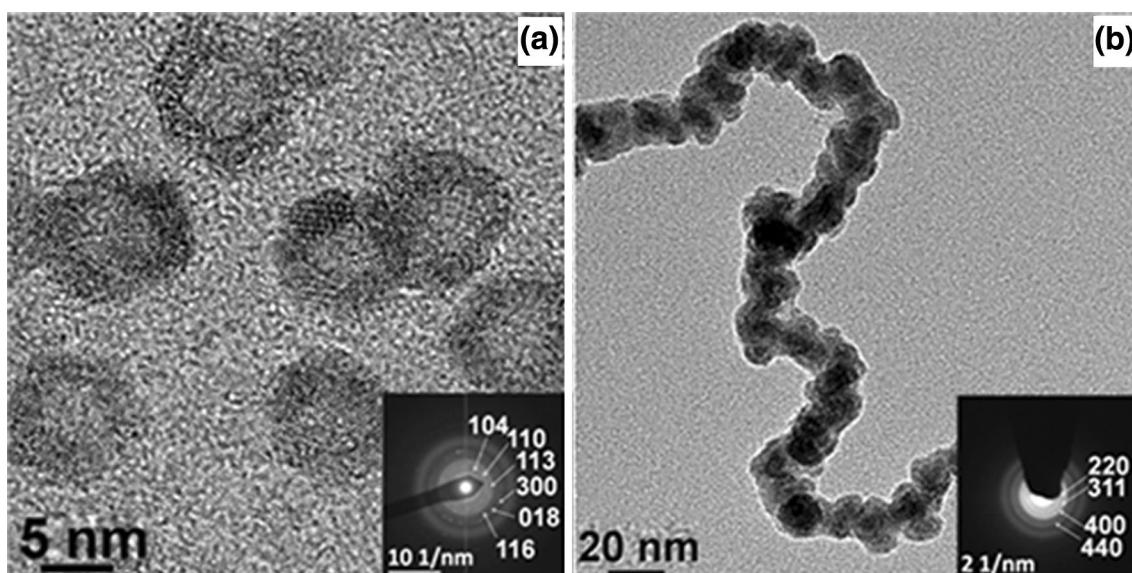


Fig. 1. TEM images of (a) hollow  $\alpha\text{-Fe}_2\text{O}_3$  NPs and (b)  $\gamma\text{-Fe}_2\text{O}_3$  nanochains from thermo-decomposing 3.50-g  $\text{Fe}(\text{CO})_5$  in 100-mL xylene with (a) 1.0-g PP-*g*-MA-1a ( $M_n \approx 8000$ ) and (b) 0.25-g PP-*g*-MA-1a. Average particle diameter (denoted as “dia”) is as follows: (a)  $\sim 7.7 \text{ nm}$  and (b)  $\sim 20.0 \text{ nm}$ . Inserts in images are the SAED patterns (Reproduce permission from John Wiley and Sons. Copyright © 2012 WILEY-VCH).<sup>14</sup>

in hydrophobic medium. Ideally, PP-g-MA is suitable for serving as a polymeric surfactant to stabilize magnetic NPs.

### Iron Oxide ( $\text{Fe}_2\text{O}_3$ ) NPs Synthesized by PP-g-MA

As shown in Fig. 1,  $\text{Fe}_2\text{O}_3$  NPs with different morphologies were achieved by simply changing the concentration of surfactant PP-g-MA-1a: monodispersed spherical hollow NPs (at high surfactant concentration) and self-assembled nanochains (at low surfactant concentration).<sup>14</sup> In addition, selected area electron diffraction (SAED) patterns (shown in the insert of Fig. 1) further confirmed

that the hollow NPs are  $\alpha$ -phase  $\text{Fe}_2\text{O}_3$ , whereas the nanochains are  $\gamma$ -phase  $\text{Fe}_2\text{O}_3$ .

A room-temperature magnetic property study further reveals a superparamagnetic behavior of the hollow  $\alpha$ - $\text{Fe}_2\text{O}_3$  NPs because no magnetic hysteresis loops (right insert of Fig. 2) were observed. In addition, the magnetization of hollow  $\text{Fe}_2\text{O}_3$  NPs did not saturate at the applied maximum magnetic field of 30 kOe, which is the characteristic of the anti-ferromagnetic  $\alpha$ -phase  $\text{Fe}_2\text{O}_3$ .<sup>18–20</sup> Upon extrapolation, the calculated saturation magnetization ( $M_s$ ) is 2.9 emu/g. On the other hand, a hard ferromagnetic behavior of the  $\text{Fe}_2\text{O}_3$  nanochains was confirmed by a clear magnetic hysteresis loop with coercivity ( $H_c$ ) of 518.0 Oe and high  $M_s$  of 54.0 emu/g (Fig. 2).

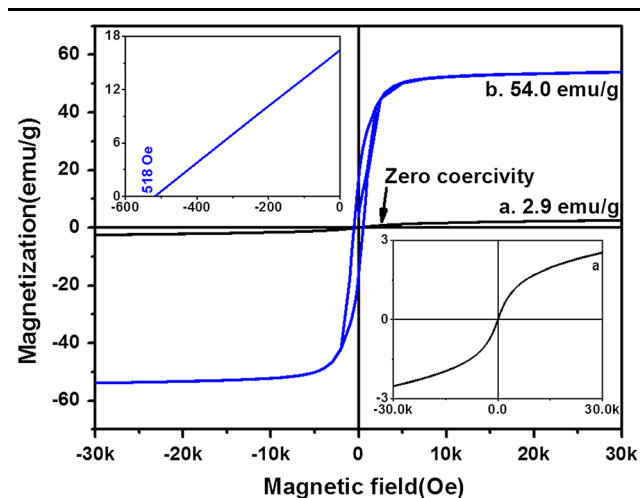


Fig. 2. Room-temperature hysteresis loops of (a)  $\alpha$ - $\text{Fe}_2\text{O}_3$  hollow NPs and (b)  $\gamma$ - $\text{Fe}_2\text{O}_3$  nanochains (Reproduce permission from John Wiley and Sons. Copyright © 2012 WILEY-VCH).<sup>14</sup>

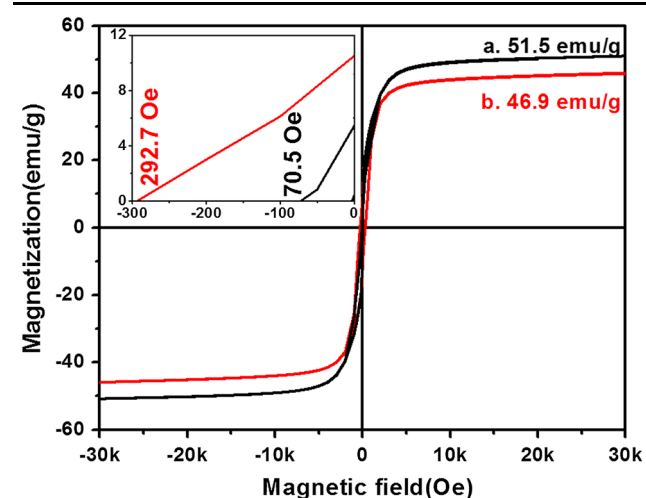


Fig. 4. Room-temperature hysteresis loops of (a) 30.0 nm and (b) 24.0 nm diameter  $\gamma$ - $\text{Fe}_2\text{O}_3$  nanochains (Reproduced by permission of The Royal Society of Chemistry).<sup>15</sup>

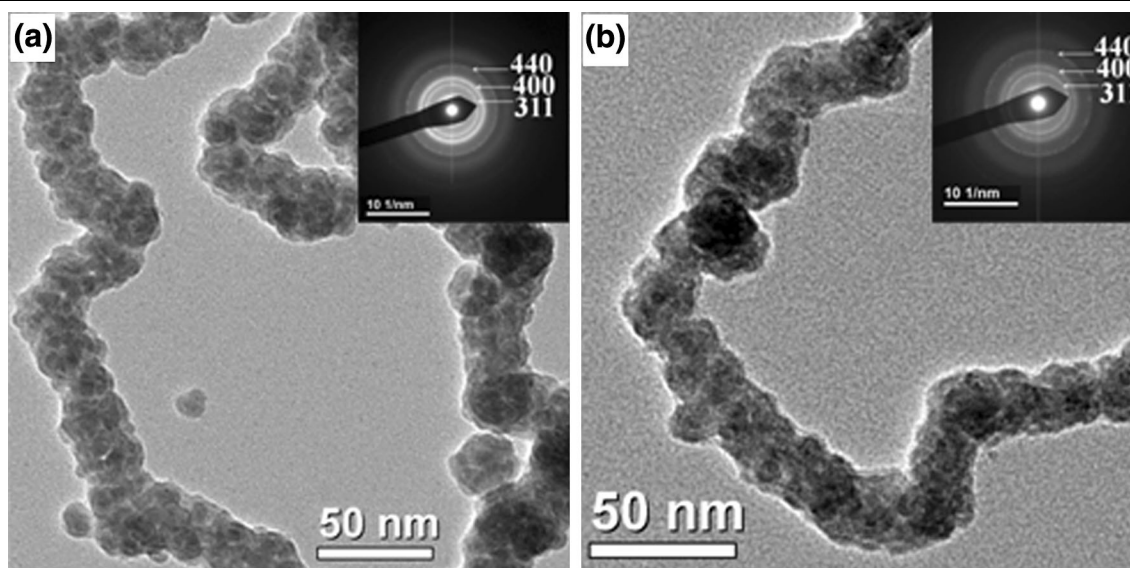


Fig. 3. TEM images of  $\gamma$ - $\text{Fe}_2\text{O}_3$  nanochains from thermo-decomposing 3.50-g  $\text{Fe}(\text{CO})_5$  in xylene with (a) 0.25-g PP-g-MA-1b ( $M_n \approx 8000$ ) and (b) 0.25-g PP-g-MA-2 ( $M_n \approx 2500$ ). Average chain diameter is as follows: (a)  $\sim 30.0$  nm and (b)  $\sim 24.0$  nm. Insets are the SAED patterns (Reproduced by permission of The Royal Society of Chemistry).<sup>15</sup>

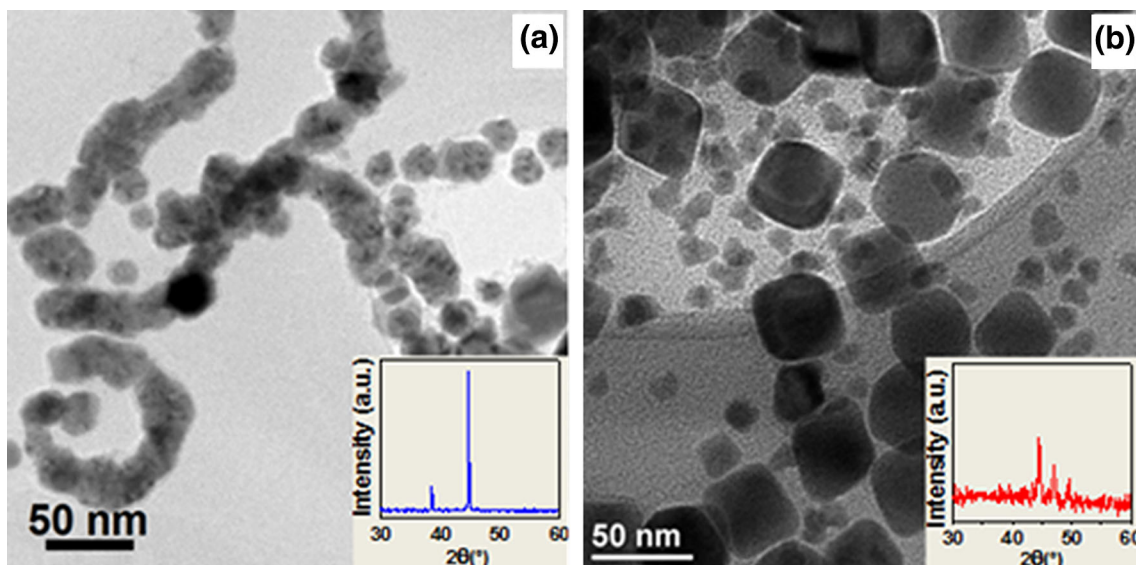


Fig. 5. TEM images of (a) fcc-phase chain-like and (b)  $\epsilon$ -phase polyhedral-shaped cobalt NPs from thermo-decomposing 5.80-g  $\text{Co}_2(\text{CO})_8$  in xylene with 7.5-g PP and (a) 0.5-g PP-*g*-MA-2 ( $M_n \approx 2500$ ) and (b) 0.5-g PP-*g*-MA-3 ( $M_n \approx 800$ ). Average particle diameter is as follows: (a)  $\sim 22.4$  nm and (b)  $\sim 40.8$  nm. Insets are XRD patterns (Reproduced by permission of The Royal Society of Chemistry).<sup>16</sup>

It can thus be concluded that the morphology, crystalline structure, and magnetic property of the as-obtained  $\text{Fe}_2\text{O}_3$  NPs can be controlled by varying PP-*g*-MA concentration upon using the same bottom-up synthesis method. The formation of the hollow NPs is caused by the nanoscale Kirkendall effect,<sup>14,21</sup> and the  $\text{Fe}_2\text{O}_3$  nanochain is formed by self-assembly of  $\gamma$ -phase  $\text{Fe}_2\text{O}_3$  NPs because the magnetic attraction forces overcome the steric hindrance forces.

When using the same PP-*g*-MA concentration (0.25 g in 100-mL xylene) while changing the PP-*g*-MA molecular weight,  $\gamma$ -phase  $\text{Fe}_2\text{O}_3$  nanochains consisted of different building block morphologies and diameters can be synthesized (shown in Fig. 3): flower-shaped nanochains versus plain nanochains with single spherical NPs. Upon investigating the intermediate stage of these nanochains, the PP-*g*-MA bonding density on the surface of the building block NPs during their nucleation and growth primarily caused the morphology changes.<sup>15</sup>

Similarly, different magnetic properties were also observed for these nanochains with different morphology. Higher  $M_s$  of the flower-shaped  $\gamma$ - $\text{Fe}_2\text{O}_3$  nanochains (diameter: 30 nm) than that of  $\gamma$ - $\text{Fe}_2\text{O}_3$  nanochains (diameter: 24 nm) was found (Fig. 4). Moreover, a soft ferromagnetic behavior for the flower-shaped nanochains was observed as evidenced by the  $H_c$  of 70.5 Oe, whereas a hard ferromagnetic behavior for the other nanochains was identified as evidenced by the  $H_c$  of 292.7 Oe. Therefore, the  $\gamma$ - $\text{Fe}_2\text{O}_3$  nanochains with different size and building block morphology can be easily controlled by only changing the molecular weight of PP-*g*-MA. For the magnetic property difference, larger shape anisotropy<sup>22</sup> for the smaller diameter

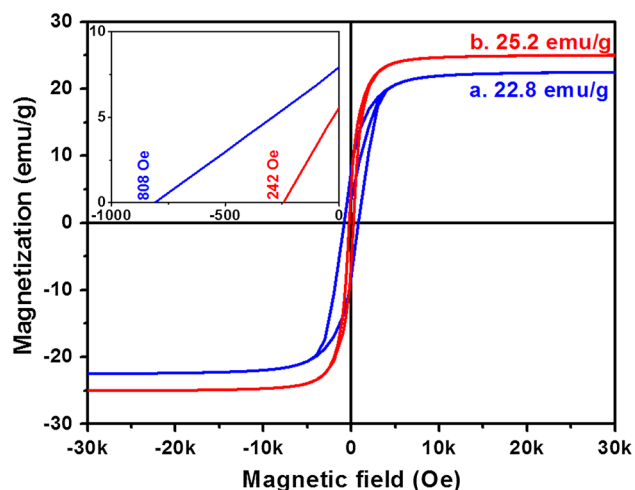


Fig. 6. Room-temperature hysteresis loops of (a) chain-like and (b) polyhedral-shaped cobalt NPs (Reproduced by permission of The Royal Society of Chemistry).<sup>16</sup>

nanochains, and the magnetization reversal mechanism<sup>23</sup> are believed to cause higher  $H_c$ .

### Cobalt NPs Synthesized by PP-*g*-MA

Cobalt (Co) NPs with different morphology (partially interconnected nanochains vs. polyhedral shape) can be obtained by varying PP-*g*-MA molecular weights during synthesizing magnetic PP/Co nanocomposites (Fig. 5). In addition, different crystalline phases (fcc- vs.  $\epsilon$ -) for these two different-shaped Co NPs were also observed as evidenced by the XRD patterns (insets of Fig. 5). The short PP-*g*-MA-3 ( $M_n \approx 800$ ) chains gave higher bonding density on the surface of Co NPs compared with the long-chain PP-*g*-MA-2, which gave stronger forces

to coordinate the growth of these NPs. Hence, the stacking sequence, the growth of a different crystal plane, and the energetics of growth<sup>8</sup> underwent different pathways that determine the final Co NPs with different sizes, shapes, and crystalline structures.<sup>16</sup>

As more MA existed in PP-g-MA-3 than in PP-g-MA-2, a higher bonding density on the surface of polyhedral-shaped  $\varepsilon$ -Co NPs resulted in stronger antioxidation than the Co nanochains, which was reflected by the higher  $M_s$  of PP composites with polyhedral-shaped NPs (25.2 emu/g) than that of the PP composites with Co nanochains (22.8 emu/g, Fig. 6). In addition, the as-prepared Co NPs with different morphologies can also cause a significant difference in  $H_c$  (inset of Fig. 6), in which the higher  $H_c$  is caused by the strong shape anisotropy from the nanochain structures.

### CONCLUSION

In summary, well-defined magnetic NPs with controllable morphologies and crystalline structures were synthesized through using modified polyolefin-PP-g-MA, which provided an alternative to the small-molecular-weight surfactants. The compatibility of PP-g-MA with many polymers can facilitate its usage for in situ preparing magnetic polymer nanocomposites with desirable physicochemical properties for a variety of applications such as magnetic resonance imaging (MRI), sensors, water treatment, and microwave shielding.

### ACKNOWLEDGEMENTS

This project is supported by Baker Hughes and a seeded Research Enhancement Grant (REG) of Lamar University. Partial support from the National Science Foundation (EAGER: CBET 11-37441 and CMMI 10-30755) is acknowledged.

### REFERENCES

1. Y. Xia, Y. Xiong, B. Lim, and S.E. Skrabalak, *Angew. Chem. Int. Ed.* 48, 60 (2009).
2. F. Dumestre, B. Chaudret, C. Amiens, M.-C. Fromen, M.-J. Casanove, P. Renaud, and P. Zurcher, *Angew. Chem. Int. Ed.* 41, 4286 (2002).
3. S. Sun and C. Murray, *J. Appl. Phys.* 85, 4325 (1999).
4. V.F. Puentes, K.M. Krishnan, and A.P. Alivisatos, *Science* 291, 2115 (2001).
5. S. Wei, Q. Wang, J. Zhu, L. Sun, H. Lin, and Z. Guo, *Nanoscale* 3, 4474 (2011).
6. L. Machala, J. Tuček, and R. Zborzil, *Chem. Mater.* 23, 3255 (2011).
7. P.R. de Moreira, A. Roldán, and F. Illas, *J. Chem. Phys.* 133, 024701 (2010).
8. D.P. Dinega and M.G. Bawendi, *Angew. Chem. Int. Ed.* 38, 1788 (1999).
9. Z. Guo, L.L. Henry, V. Palshin, and E.J. Podlaha, *J. Mater. Chem.* 16, 1772 (2006).
10. M.A. Zalich, V.V. Baranauskas, J.S. Riffle, M. Saunders, and T.G.S. Pierre, *Chem. Mater.* 18, 2648 (2006).
11. X.H. Zhang, K.M. Ho, A.H. Wu, K.H. Wong, and P. Li, *Langmuir* 26, 6009 (2010).
12. G. Liu, X. Yan, Z. Lu, S.A. Curda, and J. Lal, *Chem. Mater.* 17, 4985 (2005).
13. L.A. Miinea, B. Laura, K.D. Ericson, D.S. Glueck, and R.B. Grubbs, *Macromolecules* 37, 8967 (2004).
14. Q. He, T. Yuan, S. Wei, N. Haldolaarachchige, Z. Luo, D.P. Young, A. Khasanov, and Z. Guo, *Angew. Chem. Int. Ed.* 51, 8842 (2012).
15. Q. He, T. Yuan, X. Yan, Z. Luo, N. Haldolaarachchige, D.P. Young, S. Wei, and Z. Guo, *Chem. Commun.* 50, 201 (2014).
16. Q. He, T. Yuan, Z. Luo, N. Haldolaarachchige, D.P. Young, S. Wei, and Z. Guo, *Chem. Commun.* 49, 2679 (2013).
17. J. Rochford, D. Chu, A. Hagfeldt, and E. Galoppini, *J. Am. Chem. Soc.* 129, 4655 (2007).
18. X. Qu, N. Kobayashi, and T. Komatsu, *ACS Nano* 4, 1732 (2010).
19. S. Zeng, K. Tang, T. Li, Z. Liang, D. Wang, Y. Wang, Y. Qi, and W. Zhou, *J. Phys. Chem. C* 112, 4836 (2008).
20. K.T. Van, H.G. Cha, K.C. Nguyen, S.W. Kim, M.H. Jung, and Y.S. Kang, *Cryst. Growth Des.* 12, 862 (2012).
21. Y. Yin, R.M. Rioux, C.K. Erdonmez, S. Hughes, G.A. Somorjai, and A.P. Alivisatos, *Science* 304, 711 (2004).
22. P.M. Rao and X. Zheng, *Nano Lett.* 11, 2390 (2011).
23. B.Y. Geng, J.Z. Ma, X.W. Liu, Q.B. Du, M.G. Kong, and L.D. Zhang, *Appl. Phys. Lett.* 90, 043120 (2007).